We are IntechOpen, the world's leading publisher of Open Access books Built by scientists, for scientists

6,900
Open access books available

186,000
International authors and editors

200M
Downloads

154
Countries delivered to

Our authors are among the

TOP 1%
most cited scientists

12.2%
Contributors from top 500 universities

CLARIVATE ANALYTICS
BOOK CITATION INDEX
INDEXED

WEB OF SCIENCE™

Selection of our books indexed in the Book Citation Index
in Web of Science™ Core Collection (BKCI)

Interested in publishing with us?
Contact book.department@intechopen.com

Synchrotron Radiation-Based X-Ray Study on Energy Storage Materials

Shoaib Muhammad, Hyunchul Kim and
Won-Sub Yoon

Additional information is available at the end of the chapter

Abstract

Understanding the electrochemical processes responsible for energy storage in batteries is critical for designing of next-generation batteries. The conventional laboratory-scale characterization instruments provide limited information required for better understanding of electrochemical reaction mechanisms. Synchrotron radiations have very high brilliance and broad energy range extending from far-IR through the hard X-ray region. The availability of synchrotron radiation is driving technical and theoretical advances in scattering and spectroscopic techniques from last couple of decades. These advances in synchrotron radiation-based characterization techniques have made it possible to study the underpinning issues of energy storage materials. An electrochemical road map based on much more knowledge-driven approach can be drawn by utilizing synchrotron-based element-specific spectroscopic as well as scattering techniques. Herein, we introduce various scenarios where synchrotron radiation-based characterization methods provide inherent advantages and flexibility in obtaining detailed mechanistic information along with structural studies.

Keywords: synchrotron radiation, energy storage material, Li-ion battery, XRD, nanostructures, XAS, local structure

1. Introduction

Synchrotron radiation is emitted by charged particles, traveling at speeds relative to the speed of light when accelerated by magnetic fields. The major advantages of synchrotron radiation include very high intensity, tunable energy range, and inherently linear polarization [1]. However, one major drawback is the limited availability of the national and international

synchrotron radiation facilities. The availability of synchrotron radiation, with its characteristics of high brilliance, particular collimation, and multi-wavelength accessibility, continues to drive technical and theoretical advances in scattering and spectroscopy techniques. An exciting area being developed is the exploitation of these advances in synchrotron radiation surface and bulk-specific probe techniques to study the underpinning issues of energy storage materials.

The long-term endurance of batteries and other electrochemical devices, used in highly demanding applications like electric vehicles, is closely related to the ability of the cathode and anode materials to accommodate and release guest ions without any structural damage. A challenge in developing the understanding of energy storage process in batteries is in the direct study of the electrochemical reactions involved during battery operation. The characterization tool required needs to provide element-specific as well as overall structural information with high resolution. Synchrotron radiation-based measurements under operating conditions of batteries are critical in order to map the mechanistic causality between the local and atomic structure of functional components of batteries and their electrochemical characteristics. In this chapter, we will examine various scenarios where synchrotron radiation-based X-ray methods provide inherent advantages and flexibility in obtaining detailed mechanistic information along with structural studies.

2. Synchrotron radiation-based X-ray scattering techniques

2.1. Wide-angle X-ray scattering (WAXS)

X-ray photons interact with matter in different ways including coherent scattering, Compton scattering, photoelectric interaction, and pair production. If the interaction of the X-ray photons is coherent and elastic, the interaction is called X-ray diffraction (XRD) or Bragg scattering. A distribution of electrons in matter will interact with a photon wave to produce an interference-modulated scattering pattern, called a diffraction pattern. If multiple identical electron distributions are periodically placed in space, the scattering from each of them will interact with that from the others and will result in destructive interference in most of the direction other than a few allowed directions. These allowed directions can be calculated by considering the lattice, and hence a crystalline structure can be fully resolved by using diffraction pattern. Bragg's law is a useful model to describe the relation between the allowed scattering angles (2θ), the photon wavelength (λ), and an inter-planar distance (d) between parallel planes; see Eq. (1):

$$2d \, \sin \theta = n\lambda \qquad (1)$$

The recorded diffraction peak from a sample will have an angular width due to the broadening from the instrument. Additionally, the peaks can be broadened by the finite size of the crystallites. The peak broadening does not correlate with the particle size, but with the coherent domain length where long-range order is preserved [2]. Synchrotron radiation covers a large range of energies and that allows for superior data acquisition. In the case of XRD, it enables

the ability to probe many different crystallographic planes at the same time, resulting in fast and rich data acquisition. The use of high energy, sometimes referred to as hard X-rays, is advantageous because these X-rays are not absorbed well in a solid material and therefore allow for deep penetration. These properties of synchrotron radiation, coupled with overall high intensities, allow for rich data collection and experimentation that were previously not possible. Experimental setup for synchrotron radiation-based high-energy XRD is shown in **Figure 1**. As the high-energy photons are able to fully penetrate the cell, these measurements are conducted in the transmission mode in order to obtain 2D diffraction patterns. This also means that the cathode and anode can be investigated simultaneously.
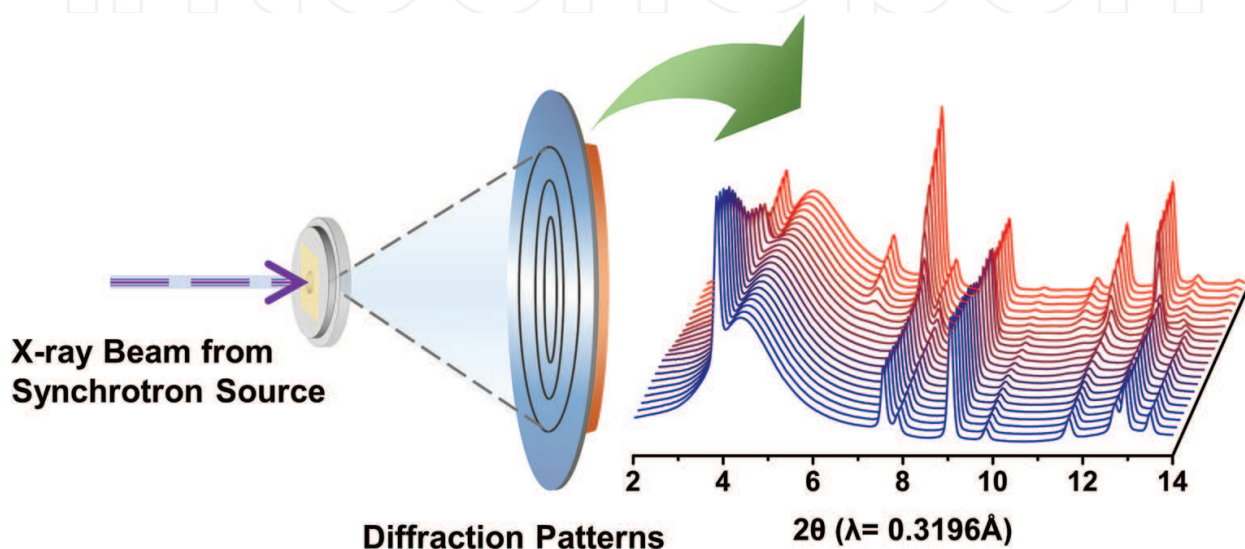

Figure 1. Schematic diagram of synchrotron radiation-based X-ray scattering technique.

2.1.1. Case study

Rechargeable Li-ion batteries are electrochemical energy storage devices of choice in portable electronics due to their high-specific energy density and now becoming increasingly popular for grid storage and electrical vehicles. In Li-ion battery, electrodes operate by reversible Li-ion insertion and extraction during charge and discharge. High-rate Li-ion battery electrode materials usually make solid solutions with Li over a large composition range in order to avoid phase transformation during (de)lithiation. Phase transformations, during cycling, are associated with small or negligible volume changes. For example, the layered compound $LiNi_{1/3}Mn_{1/3}Co_{1/3}O_2$ makes a solid solution and shows moderate volume changes; however, the high-voltage spinel $Li_x(Ni_{0.5}Mn_{1.5})O_4$ ($0 < x < 1$) shows only a small volume change (3%) for the two-phase region [3]. $LiFePO_4$, however, displays excellent high-rate performance when nanosized, despite undergoing a two-phase transformation to $FePO_4$ during delithiation, along with small volume change of 6.8% [4]. The limited Li solubility in $LiFePO_4$ and $FePO_4$ indicates that (de)lithiation occurs via a two-phase reaction, where the relative $LiFePO_4$ and $FePO_4$ amount is changed by a moving phase boundary, and not via a solid solution. The Li solubility increases by decreasing particle size, as a result of the increased interfacial energy per unit volume. By considering this interfacial energy, *ex situ*

diffraction studies of $LiFePO_4$ nanoparticles suggest that once an energetically unfavorable $LiFePO_4$-$FePO_4$ interface is formed, this interface quickly moves through the particle so as to return to the most stable $LiFePO_4$ or $FePO_4$ state, so only $LiFePO_4$ and $FePO_4$ particles are observed by *ex situ* characterization techniques.

Recently published *in situ* XRD investigations performed on micrometer-sized $LiFePO_4$ show the emergence of a metastable crystalline phase with an intermediate Li composition of $Li_{0.6-0.75}FePO_4$ when cycled at high rates [5]. Whereas, studies on nanometer-sized $LiFePO_4$ particles are limited to low [6] and moderate [7] current rates, and only small deviations in stoichiometry from $LiFePO_4$ and $FePO_4$ were observed during cycling. Due to the faster transport kinetics of nanoparticles, a high current rate is required to reach the kinetic limit of a phase transformation including an *in situ* XRD setup with high X-ray intensity and a fast read detector so that the reaction can be probed with high time resolution. By studying the nanoparticles under high current rates, Liu et al. [8] were able to force enough particles to transform simultaneously so that the reacting particles can be detected and the nature of the phase transformations that occur at an overpotential can be determined.

In situ diffraction patterns during the first five cycles of $LiFePO_4$ with an average size of 186 nm at 10 C galvanostatic charge-discharge are shown in **Figure 2(a)**. All peaks in the diffraction patterns can be indexed to either the Li-rich $Li_{1-\alpha}FePO_4$ phase or the Li-poor $Li_\beta FePO_4$ phase. During charge, peaks representing $Li_{1-\alpha}FePO_4$ phase disappear, and these peaks reappear on discharge; conversely $Li_\beta FePO_4$ peaks appear on charge and disappear on discharge. Interestingly, they observed the appearance of positive intensities between the 8.15–8.4, 13.95–14.1, and 15.15–15.4, 2θ ranges, which shows the formation of phases, in which the lattice parameters are different from those of $LiFePO_4$ and $FePO_4$. A closer view of individual diffraction patterns in selected 2θ regions is shown in **Figure 2(b)**. All of the reflections exhibit highly symmetrical profiles at the beginning of the first charge; however, the $LiFePO_4$ (2 0 0) and (3 0 1) reflections start to broaden asymmetrically toward higher angles with the charge. The most significant asymmetrical broadening is observed on discharge in patterns (*f*) and (*g*), where the (2 0 0) reflections from both phases are connected by a positive intensity band. Similar trend is observed in the second cycle as well. Neither the peak position nor the peak shape of $LiFePO_4$ is restored to that of the original state by the end of the second cycle. All selected peaks shift toward higher angle and become broad, as shown in pattern (*r*). This peak shift shows a decrease in the unit cell volume, which will in turn reduce the accessible capacity of $LiFePO_4$ at high rates. So, at the end of each cycle, the Li composition is not restored to stoichiometric $LiFePO_4$, instead a solid solution ($Li_{1-\alpha}FePO_4$) is formed with a smaller unit cell volume than that of the stoichiometric $LiFePO_4$. By using synchrotron radiation-based wide-angle X-ray scattering technique and doing further analysis like profile fitting by convoluting separate contributions from size and lattice-parameter variations with appropriate analytical functions, they further confirmed that phase transformations in nanoparticulate $LiFePO_4$ proceed, at least at high rates, via a continuous change in structure rather than a distinct moving phase boundary between $LiFePO_4$ and $FePO_4$.
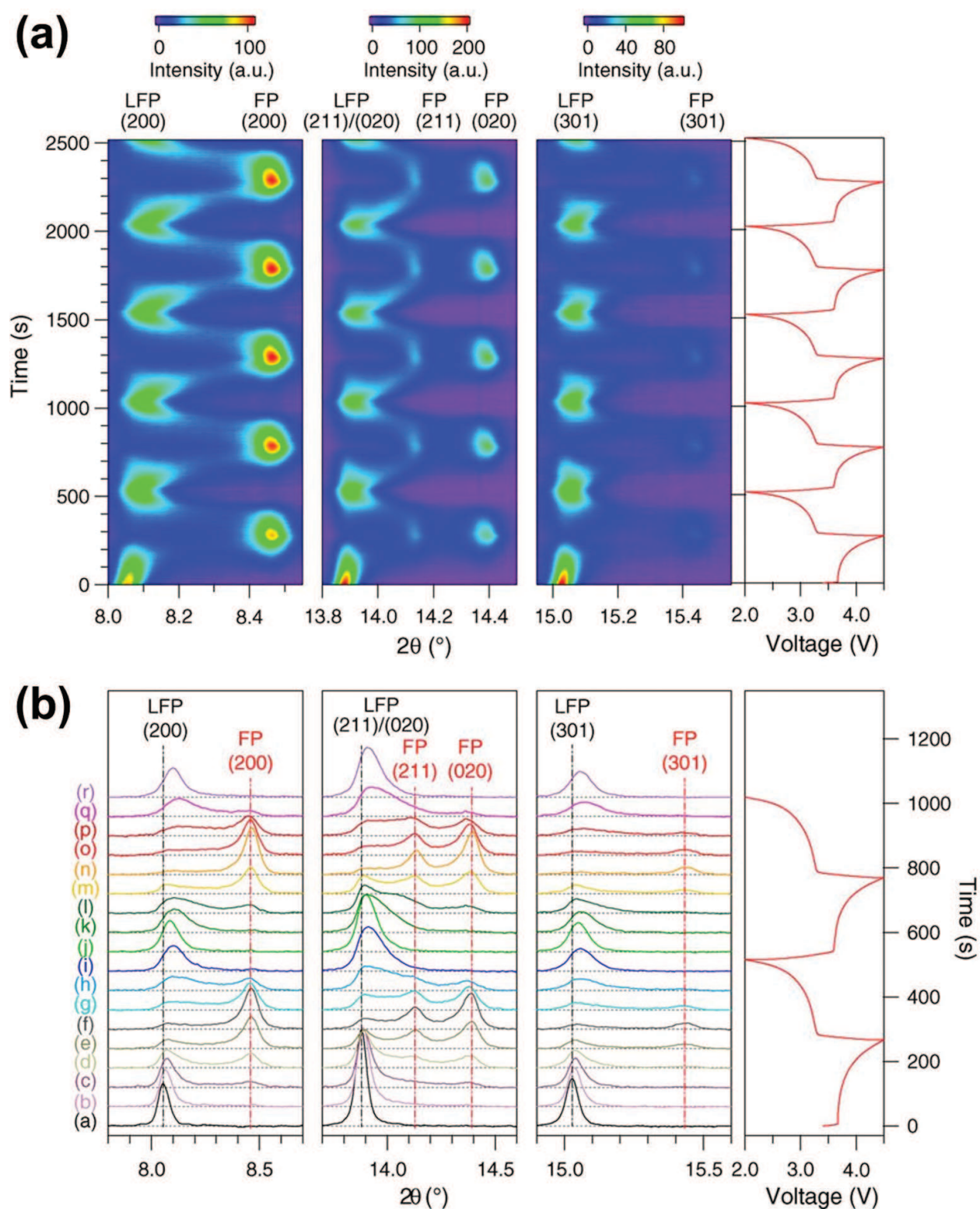
Figure 2. The variations of XRD pattern during the galvanostatic charge and discharge at a rate of 10 C. (a) The image plot of diffraction patterns for selected reflections during the first five electrochemical cycles. The corresponding voltage curve is plotted to the right. (b) Selected individual diffraction patterns during the first two electrochemical cycles stacked against the voltage profile [8].

2.2. Small-angle X-ray scattering (SAXS)

The structural characterization of nanoscale systems is a very active area of research these days not only in energy storage material system but in variety of other scientific disciplines as well. Nanoscale systems can be studied with real-space imaging or reciprocal space scattering techniques. X-ray scattering techniques provide reciprocal space data, whereas electron microscopy-based imaging techniques usually provide real-space data. A distribution of electron density at nanometer length scales will scatter an X-ray beam to low angles, while that in the atomic scale will scatter to high angles. Therefore, small-angle X-ray scattering (SAXS) is a technique to study material structures at small angles or large distances. SAXS is a powerful technique to determine, not only the object's size, size distribution, shape, surface structure, relative positions of particles, but it can also be used for the structure factor analysis. The size distribution function is a key piece of information that can be obtained from SAXS. Collected data can be fitted, when the shape of a particle is known or can be assumed, to get the size distribution. SAXS form factor analysis provides useful information at the single-particle level; the structure factor allows to figure out the organization of particle systems in the structure.

In recent years, the development of synchrotron radiation X-ray sources has made possible to adopt novel approaches to utilize X-ray scattering technique for nanoparticle research. SAXS is nondestructive and provides structural data averaged over macroscopic sample volumes. Modern synchrotron radiation-based SAXS is capable of structural characterization of sample in its working state because of its tunable flux and energy that is particularly useful for nanoparticle research especially for electrochemical energy storage systems.

2.2.1. Case study

SAXS is a useful characterizing technique for characterization of Li-ion batteries and other energy storage materials. Conventional Li-ion batteries suffer from capacity loss due to several failure mechanisms associated with the strain induced in anode and cathode materials upon electrochemical cycling. Ordered mesoporous materials have been considered as potential candidates for the next-generation electrode materials. There are several advantages associated with mesoporous electrode materials, for example, the ordered framework of mesopores which can act as a physical buffer for the volume changes, and it reduces the diffusion path length to promote easy Li and electron transport. These structures offer intrinsic high specific surface area that provides large active surface between electrolyte and electrode material. SAXS is an ideal technique to study ordered mesoporous structures. Recently, Park et al. [9] have developed an *in situ* synchrotron-based small-angle X-ray scattering (SAXS) technique to investigate the nanostructural changes of ordered mesoporous materials during cycling for further understanding the Li storage reactions.

Information on nanostructural changes of an electrode material from SAXS allows to understand fine details of nanostructured electrode dynamics during electrochemical cycling. They performed *in situ* SAXS studies on the meso-Co_xSn_y anode materials to probe the mesoscopic structural changes during its electrochemical cycling to understand the behavior of the entire electrode with different Co contents. *In situ* SAXS data including contour projection for each meso-Co_xSn_y composition during the first cycle are shown in

Figure 3. All the *in situ* SAXS patterns indicate that the present meso-Co_xSn_y materials retain highly ordered meso-structures, even though the intermetallic electrodes are known to form Li alloys during lithium insertion. There are no significant changes in the relative scattering intensities of SAXS patterns, when a discharge current is applied, until the discharge potential reaches to 0.2 V. While discharging below 0.2 V, the scattering peaks move slightly toward the lower angle, and their intensity is decreases. These results indicate that the meso-structures of all the meso-Co_xSn_y electrodes are retained until 0.2 V and then small expansion of mesoscopic cell volume and somewhat loss of meso-structural periodicity take place during the Li-Sn alloying reaction. Both the intensities and positions seem to be recovered to the initial state after the complete cycle, indicating the structural stability of meso-Co_xSn_y electrodes.
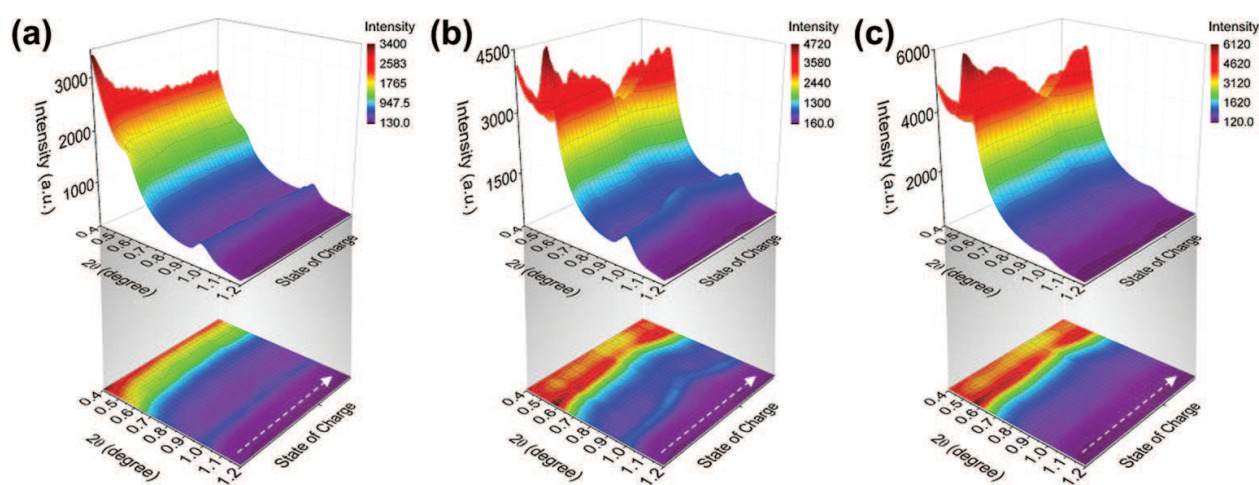

Figure 3. Color-coded 3D contours and projection maps showing SAXS data collected from ordered meso-Co_xSn_y electrodes during *in situ* experiment: (a) meso-$Co_{0.5}Sn_{0.5}$, (b) meso-$Co_{0.3}Sn_{0.7}$, and (c) meso-$Co_{0.1}Sn_{0.9}$ [9].

In order to get more insight of the *in situ* SAXS results, dQ/dV data, relative peak intensities, and mesoscopic lattice parameters were plotted against the cell voltage for the meso-Co_xSn_y electrodes as shown in **Figure 4**. This data indicates about 19% decrease of relative SAXS peak intensity and 14% expansion of meso-structural cell volume in the meso-$Co_{0.5}Sn_{0.5}$ electrode after the full discharge. In meso-$Co_{0.3}Sn_{0.7}$ electrode, there is only 13% change in the peak intensity, whereas the meso-structural cell volume expansion is 41% that is much larger than that of the meso-$Co_{0.5}Sn_{0.5}$. The initial discharge capacities of the meso-$Co_{0.3}Sn_{0.7}$ and meso-$Co_{0.5}Sn_{0.5}$ electrodes are 1321 and 822 mAh/g, respectively, due to the different amount of electroactive Sn. **Figure 4(f)** shows a significant 52% decrease in the SAXS peak intensity with relatively large volume change of 30% in the meso-$Co_{0.1}Sn_{0.9}$ electrode, while its initial discharge capacity is 1493 mAh/g. These *in situ* SAXS results for meso-Co_xSn_y electrodes during cycling directly provide roles of the inactive Co element as a chemical buffer; meanwhile, the well-defined nanoporous system acts as a physical buffer to accommodate the volume changes in the electrode. *In situ* SAXS reveals that the mesoscopic volume and meso-structural order change reversibly during cycling. It indicates that reliable nanostructure is developed and that relieves severe internal strain induced by huge volume change upon the repeated electrochemical reactions.
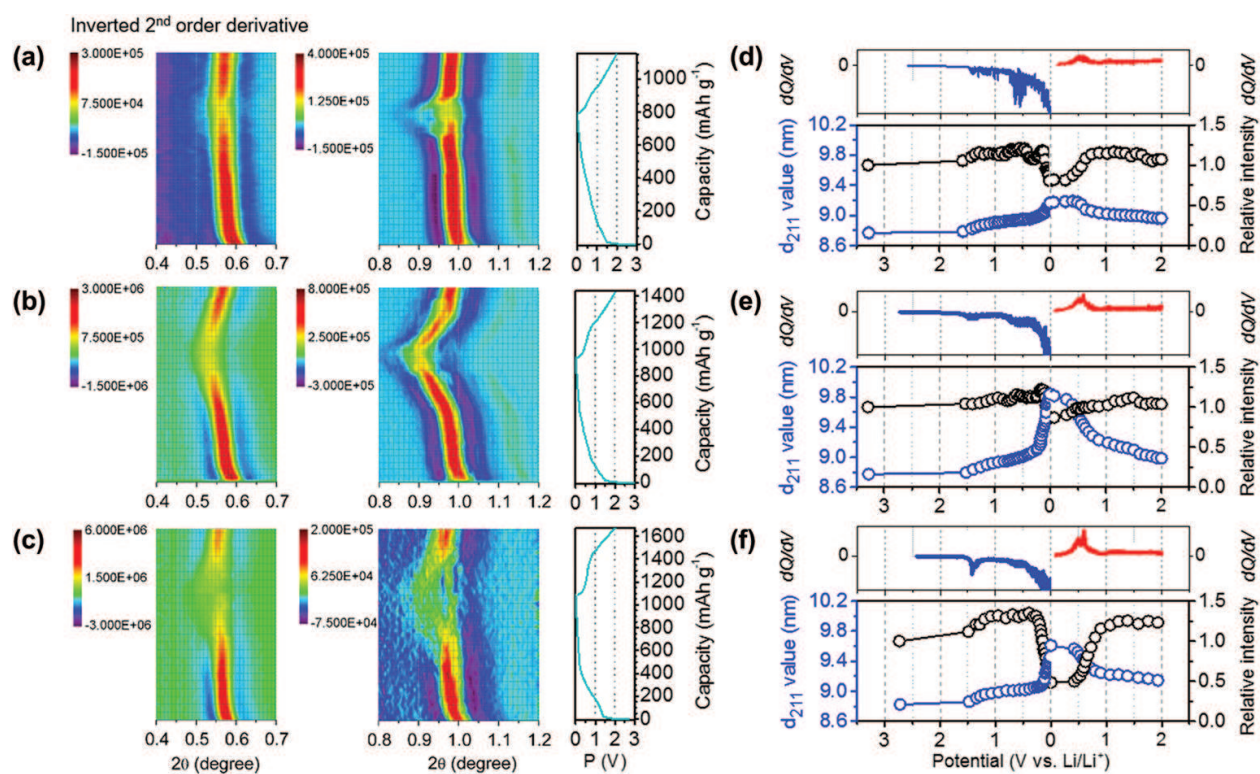
Figure 4. (a–c) Color-coded contour projection maps during *in situ* experiment with corresponding voltage profile and (d–f) the changes in lattice parameters and resolved peak-relative intensities with the corresponding dQ/dV plot for meso-$Co_{0.5}Sn_{0.5}$, meso-$Co_{0.3}Sn_{0.7}$, and meso-$Co_{0.1}Sn_{0.9}$, respectively [9].

3. Synchrotron radiation-based X-ray absorption techniques

3.1. Hard X-ray absorption spectroscopy (HXAS)

X-ray absorption spectroscopy (XAS) is a powerful technique that can characterize aII forms of matter, irrespective of their degree of crystallinity. Traditionally, diffraction-based characterization methods are being used for structural investigations, and reliable structural information can be determined for materials that exhibit a long-range structural order. In contrast XAS can probe the local structure of disordered solids, liquids, as well as amorphous materials. XAS has vast application area ranging from coordination chemistry, catalysis, biology, and surface physics to material chemistry. One of the major advantages of XAS is its atomic selectivity which makes it possible to study the local structure of each different constituent of a sample. Sample preparation for XAS is very simple, and experiments can be performed *in situ*.

XAS spectrum can be divided in two parts, namely, X-ray absorption near-edge structure (XANES) and extended X-ray absorption fine structure (EXAFS). In XANES phenomenon, an element-specific signal is generated, typically using a synchrotron radiation source. A core electron absorbs the energy of incident X-rays and gets excited beyond the Fermi level, leaving behind a core hole. The synchrotron radiation sources can provide energy that is right for desired electron transitions. When a sample is exposed to X-rays, it will absorb part of the

incoming photon beams. Other phenomena occurring are heat, X-ray fluorescence, production of unbound electrons, and of course the scattering of X-rays. The absorption of X-rays can be measured quantitatively, and it follows exponential decay given by the Beer's law [10].

The EXAFS phenomenon arises from the quantum mechanical interference of the scattering of a photoelectron by the potential of the surrounding atoms. A photoelectron emitted by the photo-absorbing atom propagates as a spherical wave and spreads out over the solid. The amplitude of all the reflected electron waves adds either constructively or destructively to the spectrum of the absorbing atom as shown in **Figure 5(a)** and **5(b)** respectively, and hence the X-ray absorption coefficient exhibits a typical oscillation. A crucial issue is the recognition that the photoelectron is not infinitely long lived; it decays as a function of time and distance, and thus the EXAFS cannot probe long-range distances. EXAFS can give only local structural information of about several angstroms around the selected atomic species.
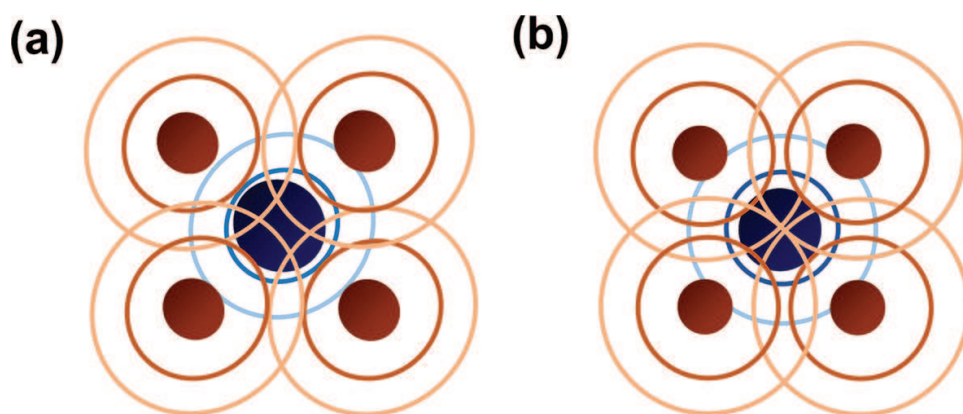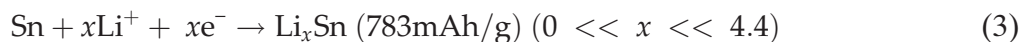

Figure 5. Constructive and destructive interference of electron wave during and XAS event.

The recent availability of high-brightness synchrotron radiation sources has resulted in a prosperous development of XAS technique, and it is finding wide application area including the energy storage material field.

3.1.1. Case study

Major challenges faced by Li-ion batteries are demand for high-energy density, capacity retention, safety, and low cost. In order to achieve the higher-energy density than that of currently commercialized ones, metal oxides are being considered as potential anode materials due to their high-energy density arising from conversion and alloying reactions [11]. SnO_2 is a candidate anode material for future batteries, and previous studies show that SnO_2 anode undergoes an irreversible conversion reaction in the initial cycle followed by a reversible alloying reaction of Sn [12, 13]:

$$SnO_2 + 4Li^+ + 4e^- \rightarrow Sn + 2Li_2O \quad (711\,mAh/g) \tag{2}$$

$$Sn + xLi^+ + xe^- \rightarrow Li_xSn \ (783mAh/g) \ (0 \ << \ x \ << \ 4.4) \tag{3}$$

Reaction based on Eq. (2) is the main reason for initial irreversible capacity of this anode material, whereas reaction based on Eq. (3) is responsible for reversible capacity of these electrode materials in the subsequent cycles. Surprisingly, reported capacity of nanostructured SnO_2-based anode materials is higher than the abovementioned theoretical capacity (783 mAh/g). To understand this anomalous capacity, Kim et al. [14] conducted the synchrotron-based XAS experiments on mesoporous SnO_2 anode material. The combination of XRD and XAS was used to probe the bulk and local structure. The XRD peaks almost disappeared (not shown here) after discharging below 0.7 V indicating that mesoporous SnO_2 converts to an amorphous nano-Li_xSnO_2 phase, so XRD alone was unable to further characterize this material.

Figure 6(a) shows selected Sn K-edge XANES and EXAFS patterns in the initial discharge region of the first cycle. The oxidation state of Sn in the mesoporous SnO_2 is 4+. The reduction of Sn takes places in the beginning of discharge, and the Sn K-edge XANES spectra show prominent shift toward lower-energy values. This reduction of Sn during conversion reaction effects the local environment around the Sn atom. The first prominent peak in Sn K-edge EXAFS spectra corresponds to the Sn-O interaction in the first coordination shell, and the broad peaks in 2.2–3.9 Å region are due to the Sn-Sn, Sn-O, and Sn-Sn interactions in the subsequent coordination shells. The intensity of these peaks decrease significantly during discharge due to displacement of reacting species during the conversion reaction. **Figure 6(b)** shows XAS data obtained in the middle discharge region of the first cycle. In this region, Sn K-edge XANES spectra show only negligible shift toward lower-energy values. However, Sn K-edge intensities decrease in this region, showing the formation of metallic Sn. After discharging beyond 600 mAh/g, the intensity of the Sn-O peak decreases, a new peak at around 2.6 Å emerges, which corresponds to the Sn-Sn(Li) pair in the Li_xSn alloy, and the intensity of this new peak increases with the increase of the Li/Sn ratio. The intensity of the peaks representing the Sn-O peaks gradually drops, and that of the Sn-Sn(Li) peak increases during this discharge region. The representative peaks for Sn-O bond disappear when the discharge capacity reaches 1500 mAh/g, which shows the completion of the conversion reaction. So, the remaining discharge capacity can be assigned to the alloying reaction only. **Figure 6(c)** shows the XAS data obtained from the mesoporous SnO_2 electrode in the last discharge region of the first cycle. XANES data obtained in this discharge region show a shift toward high energy of the Sn K-edge. During the alloying reaction, charge redistribution takes place to minimize the electrostatic energy which results in shifts of Sn K-edge. In the EXAFS spectra, the amplitude of the Sn-Sn peak continuously decreases in this discharge region. Due to increase in the Li/Sn ratio, the amount of Li around Sn increases. Li has a much smaller electron-scattering cross section compared to Sn. So, the intensity of the Sn-Sn(Li) peak decreases when the Li/Sn molar ratio exceeds 3 [15]. This trend of XANES and EXAFS data suggests that the capacity in this deep discharge region is obtained only by Li alloying in the Li_xSn phase until it achieves its nominal composition of $Li_{4.4}Sn$.
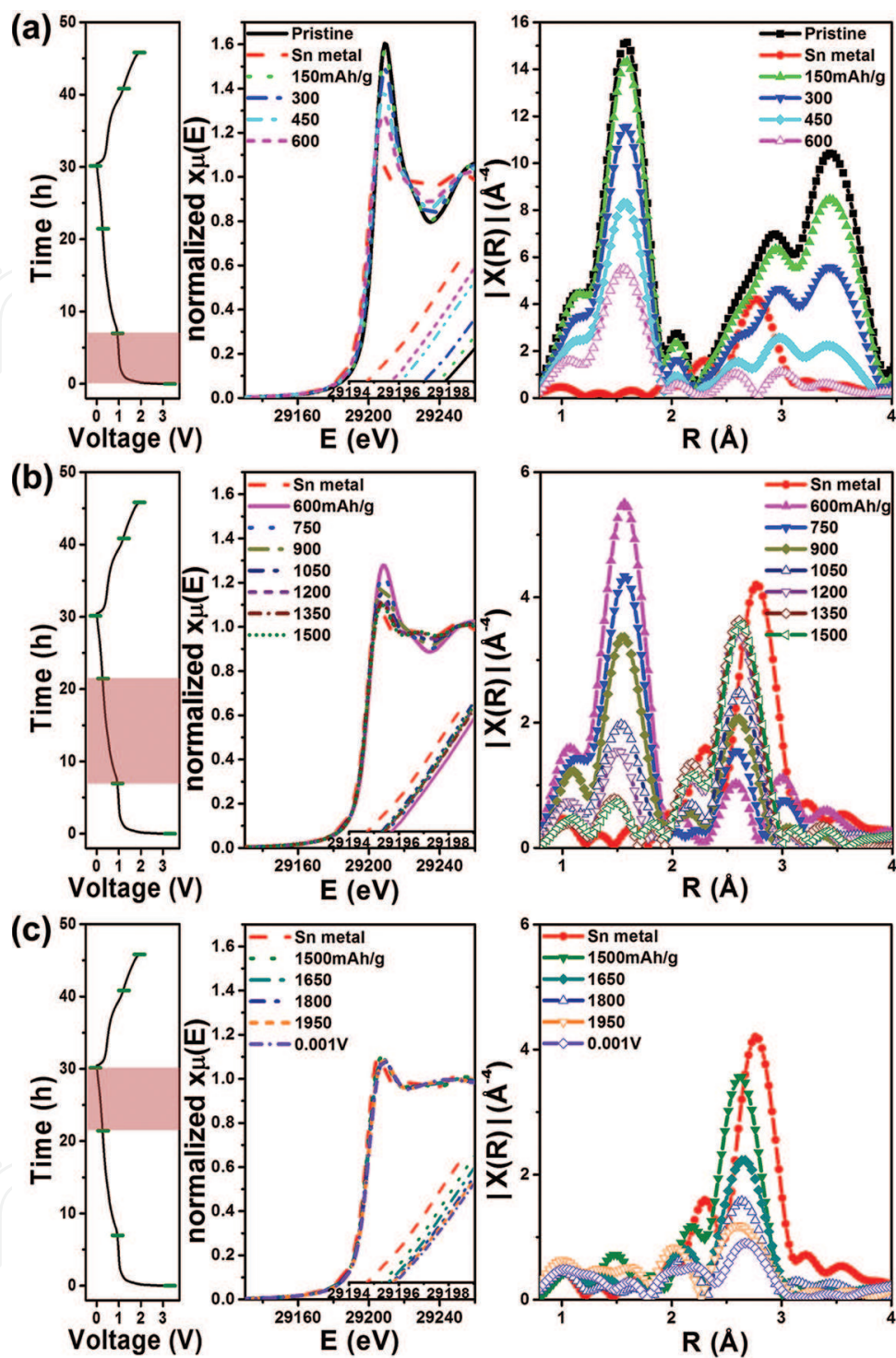
Figure 6. Sn K-edge XANES and EXAFS spectra with corresponding voltage profile taken in (a) the first discharge region, (b) the middle discharge region, and (c) the last discharge region of the first cycle [14].

Figure 7(a) shows XAS data taken from the mesoporous SnO$_2$ electrode in the beginning of charge. The Sn K-edge XANES spectra shift reversibly toward lower-energy values, and EXAFS spectra show the rise of Sn-Sn(Li)-related peaks, suggesting that the dealloying

reaction is taking place in this voltage region. After the cell was charged to 500 mAh/g, the intensity of the Sn-Sn(Li) peaks starts to decrease and that of Sn-O peak increases, as shown in **Figure 7(b)**. Appearance of the Sn-O peak and damping of the Sn-Sn peak are only possible when Li_2O formation is at least partially reversible, along with the formation of the SnO_x phase. These results suggest that the reversible charge capacity at the end of the charge can be assigned to dealloying of Li_xSn phase as well as the conversion reaction of Sn into the SnO_x phase. After achieving charge capacity of 900 mAh/g, peaks representing the Sn-O coordination shell grow with small change of the Sn-Sn peak, indicating that reversible charge capacity is mainly achieved by conversion reaction in this region. XANES spectra do not show noticeable shift in this charge region. The overall EXAFS data in the first cycle show that active material in SnO_2 does not come back to its initial composition after one complete electrochemical cycle; it changes into metallic Sn with a small quantity of amorphous SnO_x along with Li_xSn phase. In short, local structure analyses via hard XAS technique successfully demonstrated the origin of high capacity of mesoporous SnO_2 beyond its reported theoretical capacity.
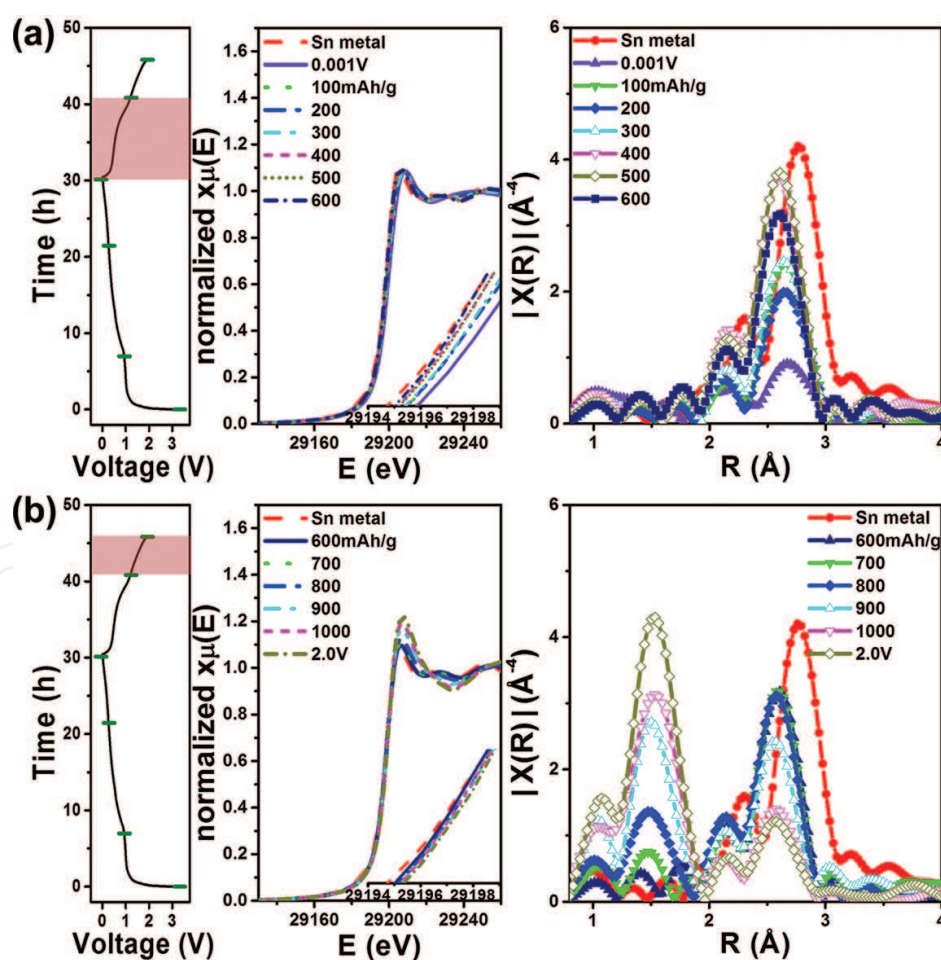

Figure 7. Sn K-edge XANES and EXAFS spectra with corresponding voltage profile taken in (a) the first charge region and (b) the last charge region of the first cycle [14].

3.2. Soft X-ray absorption spectroscopy (SXAS)

Soft XAS is an XAS technique that uses soft X-rays, with energies ranging from 150 to 1200 eV. This energy range covers the K-edge of light elements, for example, B, C, N, O, and F, along with the $L_{2,3}$ edges of the first-row transition metal elements. In an XAS experiment, tunable X-rays hit the sample and 1s electrons are ejected when the X-ray reaches a specific energy, such as the K-edge energy of oxygen (532 eV). The resulting core hole is relaxed either by transfer of electron from higher levels into the core hole which leads to the emission of fluorescent X-rays or by releasing the Auger electrons. A schematic diagram of the core hole relaxation process is shown in **Figure 8**. Both the fluorescent X-rays and the Auger electron signals can be utilized to get XAS spectra as both the signals are proportional to the incident X-ray absorption. The fluorescent X-rays possess higher escape depth of about 2000 Å, contrary to the Auger electrons, which have an escape depth of only about 50 Å. Because of this difference in escape depths, different information can be collected from fluorescent X-rays and Auger electrons. The fluorescent X-ray signal is more sensitive about the bulk structure, whereas the Auger electron yield is responsive for the surface structure. By measuring fluorescent and electron yields simultaneously, information about both surface and bulk can be obtained in the same experiment [16].
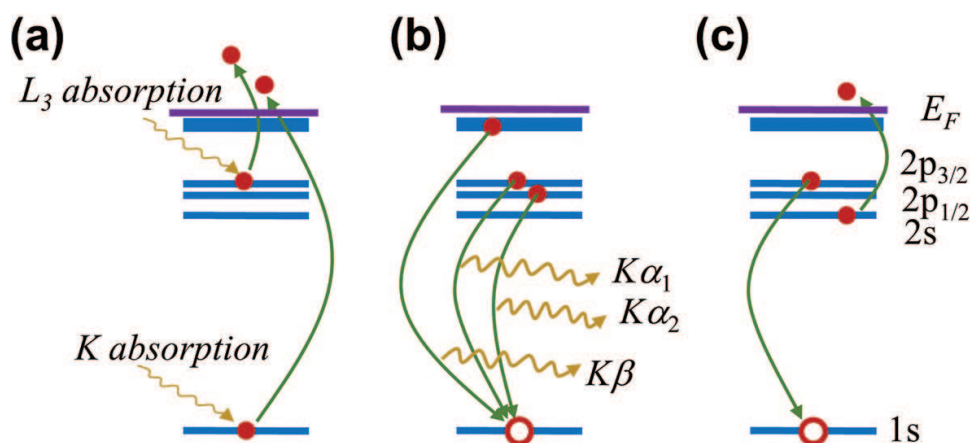

Figure 8. Schematic diagram of principle of (a) absorption, (b) fluorescent, and (c) Auger electron-yield soft X-ray absorption spectroscopy.

3.2.1. Case study

Thermal stability is a critical issue related to the safety of the rechargeable batteries. Traditionally, it is studied by using thermo-analytical techniques like TGA, or there are some studies by using *in situ* XRD. Yoon et al. utilized *in situ* temperature-dependent soft XAS measurements for the first time, in order to understand the role of different transition metals in thermal degradation of the charged $LiNi_{0.8}Co_{0.15}Al_{0.05}O_2$ electrode [17]. They monitored the element-selective structural changes in the charged cathode material on the surface and in the bulk during heating of electrode material. The findings of their study provide important guidelines to design new electrode materials with enhanced thermal safety.

Normalized Ni L-edge spectra of $Li_{0.33}Ni_{0.8}Co_{0.15}Al_{0.05}O_2$ cathode using fluorescent yield (FY) mode at various temperatures are shown in **Figure 9(a)**, and the partial electron yield (PEY)

mode spectra are shown in **Figure 9(b)**. Due to spin-orbit interaction of the core hole, the absorption spectrum splits into two energy bands, Ni $2p_{3/2}$ (L_3 edge) and Ni $2p_{1/2}$ (L_2 edge). Changes in energy position of these bands can indicate valence-state variations during the heating process as energy position shifts about 1 eV per oxidation-state change [18]. Ni L_3 and L_2 spectra obtained in the bulk sensitive fluorescent yield mode do not show energy position changes. $Li_{0.33}Ni_{0.8}Co_{0.15}Al_{0.05}O_2$ material is based on layered structure with $R\overline{3}m$ space group, and the change into the $Fd3m$ structure during heating would not involve a valence-state change or shift in energy position of L-edges. However, the energy position of Ni L_3 and L_2 spectrum moves to lower-energy values in case of surface-sensitive electron yield mode, and a rather prominent shift takes place at around 200°C that shows the presence of a NiO-type rock salt structure on the surface at this temperature. **Figure 9(c)** and **(d)** shows normalized Co L-edge XAS spectra at various temperatures using FY and PEY mode, respectively. Unlike the Ni L-edge spectra, the electron-yield spectra of the Co species do not show energy shifts. There are no visible changes in both the FY and the PEY spectra which show that cobalt ions have better thermal stability compared to the nickel ions. Partial substitution of nickel by cobalt in the cathode materials enhances its thermal stability.
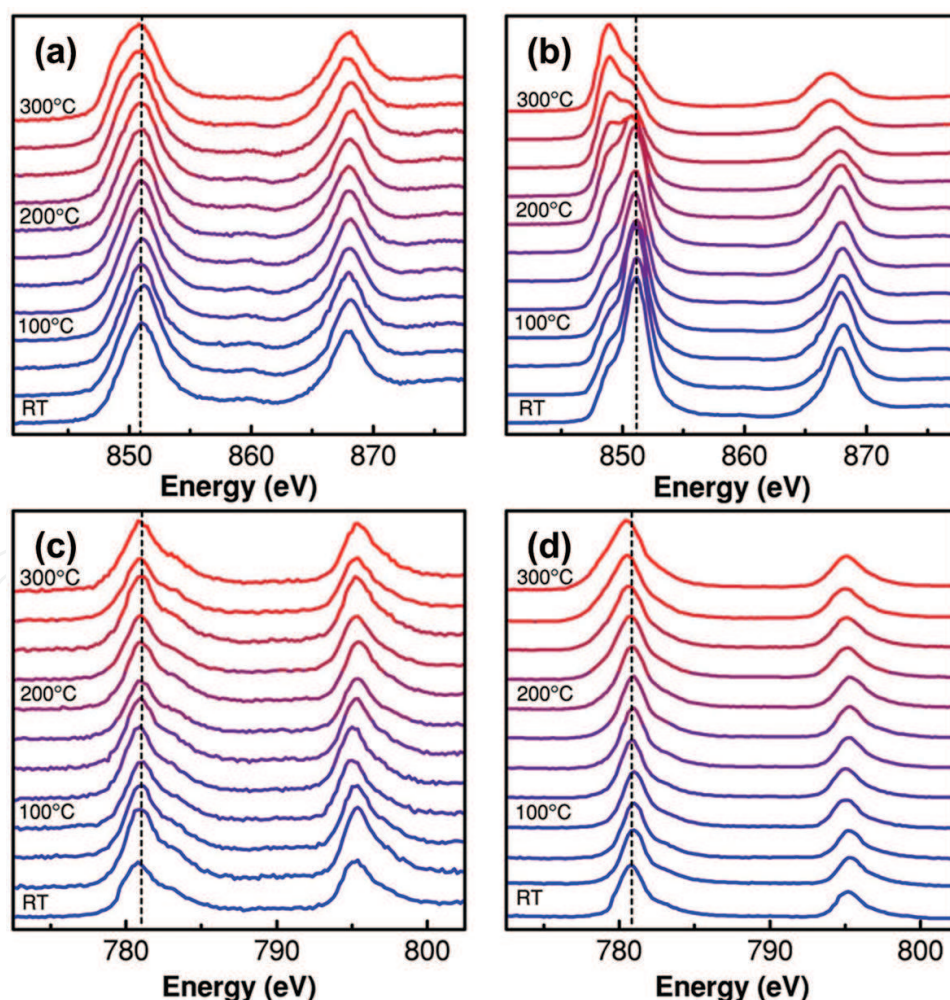

Figure 9. Normalized XAS spectra of $Li_{0.33}Ni_{0.8}Co_{0.15}Al_{0.05}O_2$ cathode material at different temperatures using (a) Ni L-edge FY mode, (b) Ni L-edge PEY mode, (c) Co L-edge FY mode, and (d) Co L-edge PEY mode [17].

Figure 10 shows the normalized O K-edge XAS spectra of $Li_{0.33}Ni_{0.8}Co_{0.15}Al_{0.05}O_2$ cathode material at various temperatures, using FY mode and PEY mode. The first prominent absorption peak at 528.5 eV corresponds to transition from oxygen 1s orbital to a hybridized state of metal 3d-O 2p orbitals. The oxygen K-edge spectra contain information associated with transitions to hybridized states of O 2p-Ni 4sp and other empty orbitals in that energy region. Like the L-edge spectra, there is no significant change in the fluorescence-yield spectra, but the surface-sensitive electron-yield spectra show a significant decrease of the peak at 528.5 eV when temperature rises above 200°C. The PEY data show other distinct differences as well. The intensity of the distinct peak at ~534 eV is decreasing, whereas that of the peak at ~532 eV is increasing with rising temperature. The features at around 532 eV and 534 eV are associated with the presence of NiO and Li_2CO_3, respectively, as shown by the spectra of the standards in **Figure 10(b)**. Upon heating, intensity of the features at 534 eV decreases which suggests that carbonate present on the surface is gradually decomposed. Conversely, the intensity of the 532 eV peak increases with temperature, particularly above 200°C, and the intensity of the 528.5 eV peak decreases. These observations indicate the formation of reduced divalent nickel oxide. This finding is in accordance with the Ni L-edge measurements. The presence of NiO-type rock salt structure and its increased formation at electrode surface with increasing temperature indicates nickel oxides tend to release oxygen at higher temperature. The oxygen K-edge spectra are consistent with the data obtained from the Ni L-edge and point toward the initiation of thermal reduction reactions around Ni sites on the surface of the cathode sample material.
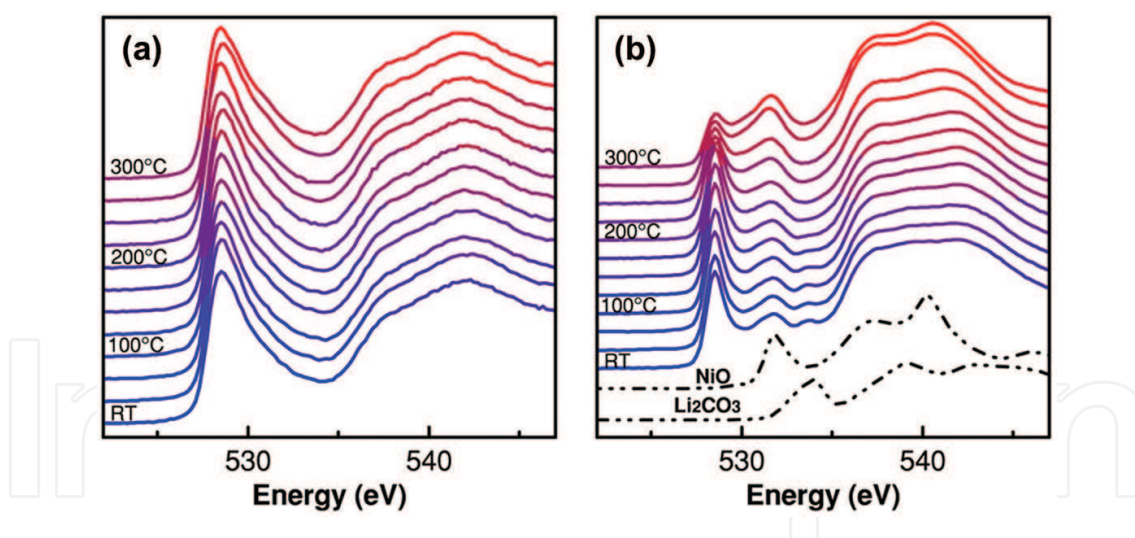

Figure 10. Normalized O K-edge XAS spectra of $Li_{0.33}Ni_{0.8}Co_{0.15}Al_{0.05}O_2$ cathode material at different temperatures using (a) FY mode and (b) PEY mode [17].

These investigations demonstrated the capability of *in situ* soft XAS techniques to investigate thermal behavior of cathode materials and show that there is no valence-state change in the bulk despite the layered structure of the $Li_{0.33}Ni_{0.8}Co_{0.15}Al_{0.05}O_2$ cathode material converts to spinel structure. The surface-sensitive PEY measurements reveal that this electrode material loses oxygen at high temperatures leading to a lower oxidation state of Ni and formation of NiO-like rock salt structure. No evidence of a surface reaction near Co sites in the investigated

temperature range was found which shows that the Co is more stable at elevated temperatures compared to the Ni in $Li_{0.33}Ni_{0.8}Co_{0.15}Al_{0.05}O_2$. The capability of soft XAS to discriminate the surface and bulk electronic structures with element specificity makes it a valuable addition to the advanced synchrotron-based characterization technique that help understand thermal behavior of battery electrodes.

4. Conclusion

The application of synchrotron-based characterization techniques to investigate energy storage materials is playing a major role in the fundamental understanding of the electrochemical reaction mechanism of energy storage materials. This chapter provides an overview about various X-ray synchrotron-based characterization techniques and their applications to electrode materials to characterize the nano- and mesoporous phase dynamics, long-range crystal order, and local and electronic changes during the electrochemical cycling of electrode materials. The combination of these techniques can provide critical information to reveal the electrochemical reaction mechanism and functional properties of electrode materials in order to better understand the existing energy storage systems and help design modern electrode materials for future applications. Given the recent developments, it can be expected that application of synchrotron-based characterization techniques will become increasingly important in development of high-performance and stable energy storage materials.

Acknowledgements

Author details

Shoaib Muhammad, Hyunchul Kim and Won-Sub Yoon*

*Address all correspondence to: wsyoon@skku.edu

Department of Energy Science, Sungkyunkwan University, Suwon, South Korea

References

[1] N. A. Young. The application of synchrotron radiation and in particular X-ray absorption spectroscopy to matrix isolated species. Coordination Chemistry Reviews. 2014;**277–278**:224–274. DOI: 10.1016/j.ccr.2014.05.010

[2] M. Ladd, R. Palmer. X-rays and white radiation. In: M. Ladd and R. Palmer, editors. Structure Determination by X-ray Crystallography. 5th ed. Springer Science+Business Media New York: Springer US; 2013. pp. 111–159. DOI: 10.1007/978-1-4614-3954-7_3

[3] M. Kunduraci, G. G. Amatucci. Synthesis and characterization of nanostructured 4.7 V $Li_xMn_{1.5}Ni_{0.5}O_4$ spinels for high-power lithium-ion batteries. Journal of the Electrochemical Society. 2006;**153**(7):A1345–A1352. DOI: 10.1149/1.2198110

[4] A. K. Padhi, K. S. Nanjundaswamy, J. B. Goodenough. Phospho-olivines as positive-electrode materials for rechargeable lithium batteries. Journal of the Electrochemical Society. 1997;**144**(4):1184–1194. DOI: 10.1149/1.1837571

[5] Y. Orikasa, T. Maeda, Y. Koyama, H. Murayama, K. Fukuda, H. Tanida, H. Arai, E. Matsubara, Y. Uchimoto, Z. Ogumi. Direct observation of a metastable crystal phase of $LixFePO_4$ under electrochemical phase transition. Journal of American Chemical Society. 2013;**135**(15):5497–5500. DOI: 10.1021/ja312527x

[6] Y. Orikasa, T. Maeda, Y. Koyama, H. Murayama, K. Fukuda, H. Tanida, H. Arai, E. Matsubara, Y. Uchimoto, Z. Ogumi. Transient phase change in two phase reaction between $LiFePO_4$ and $FePO_4$ under battery operation. Chemistry of Materials. 2013;**25**(7):1032-1039. DOI: 10.1021/cm303411t

[7] N. Sharma, X. Guo, G. Du, Z. Guo, J. Wang, Z. Wang, V. K. Peterson. Direct evidence of concurrent solid-solution and two-phase reactions and the nonequilibrium structural evolution of $LiFePO_4$. Journal of American Chemical Society. 2012;**134**(18):7867–7873. DOI: 10.1021/ja301187u

[8] H. Liu, F. C. Strobridge, O. J. Borkiewicz, K. M. Wiaderek, K. W. Chapman, P. J. Chupas, C. P. Grey. Capturing metastable structures during high-rate cycling of $LiFePO_4$ nanoparticle electrodes. Science. 2014;**344**(6191):1480–1487. DOI: 10.1126/science.1252817

[9] G. O. Park, J. Yoon, J. K. Shon, Y. S. Choi, J. G. Won, S. B. Park, K. H. Kim, H. Kim, W. S. Yoon, J. M. Kim. Discovering a dual-buffer effect for lithium storage: durable nanostructured ordered mesoporous Co-Sn intermetallic electrodes. Advanced Functional Materials. 2016;**26**(17):2800–2808. DOI: 10.1002/adfm.201600121

[10] D. F. Swinehart. The Beer-Lambert Law. Journal of Chemical Education. 1962;**39**(7):333–335. DOI: 10.1021/ed039p333.

[11] W. J. Zhang. A review of the electrochemical performance of alloy anodes for lithium-ion batteries. Journal of Power Sources. 2011;**196**(1):13–24. DOI: 10.1016/j.jpowsour.2010.07.020

[12] I. A. Courtney, J. R. Dahn. Electrochemical and *in situ* X-ray diffraction studies of the reaction of lithium with tin oxide composites. Journal of the Electrochemical Society. 1997;**144**(6):2045–2052. DOI: 10.1149/1.1837740

[13] I. A. Courtney, J. R. Dahn. Key factors controlling the reversibility of the reaction of lithium with SnO_2 and Sn_2BPO_6 glass. Journal of the Electrochemical Society. 1997;**144**(9):2943–2948. DOI: 10.1149/1.1837941

[14] H. Kim, G. O. Park, Y. Kim, S. Muhammad, J. Yoo, M. Balasubramanian, Y. H. Cho, M. G. Kim, B. J. Lee, K. S. Kang, H. S. Kim, J. M. Kim, W. S. Yoon. New insight into the reaction mechanism for exceptional capacity of ordered mesoporous SnO_2 electrodes via synchrotron-based X-ray analysis. Chemistry of Materials. 2014;**26**(22):6361–6370. DOI: 10.1021/cm5025603

[15] A. N. Mansour, S. Mukerjee, X. Q. Yang, J. McBreen. *In situ* X-ray absorption and diffraction study of the Li reaction with a tin composite oxide glass. Journal of the Electrochemical Society. 2000;**147**(3):869–873. DOI: 10.1149/1.1393284

[16] J. McBreen. The application of synchrotron techniques to the study of lithium-ion batteries. Journal of Solid State Electrochemistry. 2009;**13**(7):1051–1061. DOI: 10.1007/s10008-008-0685-1

[17] W. S. Yoon, O. Haas, S. Muhammad, H. Kim, W. Lee, D. Kim, D. A. Fischer, C. Jaye, X. Q. Yang, M. Balasubramanian, K. W. Nam. *In situ* soft XAS study on nickel-based layered cathode material at elevated temperatures: a novel approach to study thermal stability. Scientific Reports. 2014;**4**(6827):1–5. DOI: 10.1038/srep06827

[18] H. Wang, D. S. Patil, W. Gu, L. Jacquamet, S. Friedrich, T. Funk, S. P. Cramer. L-edge X-ray absorption spectroscopy of some Ni enzymes: probe of Ni electronic structure. Journal of Electron Spectroscopy and Related Phenomena. 2001;**114**–**116**:855–863. DOI: 10.1016/S0368-2048(00)00370-4